Methods 241 (2025) 173–183

Contents lists available at ScienceDirect

Methods

journal homepage: www.elsevier.com/locate/ymeth

Inside the cell: Approaches to evaluating mRNA internalization and trafficking☆

Claudia Del Toro Runzer [a], Christian Plank [b], Martijn van Griensven [a,c], Elizabeth R. Balmayor [c,d,*,1]

[a] Department of Cell Biology-Inspired Tissue Engineering, MERLN Institute for Technology-Inspired Regenerative Medicine, Maastricht, Limburg 6229 ER, the Netherlands
[b] Ethris GmbH, Planegg, Bavaria 82152, Germany
[c] Musculoskeletal Gene Therapy Laboratory, Rehabilitation Medicine Research Center, Mayo Clinic, Rochester, MN 55905, USA
[d] Experimental Orthopedics and Trauma Surgery, Department of Orthopedics, Trauma, and Reconstructive Surgery, RWTH Aachen University Hospital, 52074 Aachen, Germany

ARTICLE INFO

Keywords:
mRNA
Cellular uptake
Correlative light and electron microscopy
Transfer to lysosomes
Endocytic pathways

ABSTRACT

With the growing prominence of mRNA-based therapeutics and vaccines, accurately assessing the cellular uptake of mRNA complexes is a critical first step in evaluating both the efficiency of delivery systems and their downstream therapeutic potential. This is especially important when working with novel mRNA constructs, comparing different delivery vectors, or targeting diverse cell types. In this study, we present a suite of methods to quantify and visualize mRNA internalization following transfection of three types of human primary cells: mesenchymal stromal cells, fibroblasts, and osteoblasts. We highlight the utility of fluorescent probes for both qualitative and quantitative assessment of mRNA uptake and intracellular trafficking. To dissect the pathways involved in uptake, we employed three distinct endocytic inhibitors—chlorpromazine, wortmannin, and genistein—each targeting specific endocytic mechanisms. Additionally, we provide protocols for the lipid-based transfection agents Lipofectamine 3000 and 3DFect, which can be adapted for use with similar vectors. Key methodologies such as flow cytometry and correlative light and electron microscopy, known as CLEM, are described in detail for their effectiveness in analyzing mRNA internalization. A deeper understanding of the internalization and intracellular fate of mRNA is essential for the advancement of more efficient and safer mRNA-based delivery platforms.

1. Introduction

Due to the large molecular size of mRNA, its negative charge, hydrophilicity, and fragile nature, this molecule can rarely cross the cellular membrane by diffusion [1]. Moreover, the rapid degradation of naked mRNA in both extracellular and intracellular environments by endo- and *exo*-ribonucleases (RNases), substantially impairs the efficiency and persistence of mRNA-mediated protein expression [2]. Overcoming these barriers requires the use of specialized delivery systems capable of safely and efficiently transporting therapeutic mRNA to the ribosomes in the cytoplasm. The rapid and evolving field of nanotechnology has designed a wide range of mRNA carriers, ranging from lipid and polymeric particles, organic and inorganic materials, and hybrid compounds [3]. However, cellular uptake of these carriers does not guarantee successful protein translation, as mRNA complexes frequently become trapped in endolysosomal compartments, where they are subject to degradation before reaching the cytosol [4].

Assessing the efficacy of a certain mRNA and its delivery method begins with investigating the cellular uptake of the mRNA complex. Understanding mRNA bioavailability to host cells and its impact on *in situ* protein production is crucial. This study outlines two complementary approaches to evaluate cellular uptake and trafficking of mRNA complexes. First, we present quantitative analysis using flow cytometry, which enables precise measurement of mRNA uptake across large cell

☆ This article is part of a special issue entitled: 'Editors Collection - YMETH' published in Methods.

* Corresponding author at: Head of Experimental Orthopedics and Trauma Surgery, Department of Orthopedics, Trauma and Reconstructive Surgery, RWTH Aachen University Hospital, 2020, 52074 Aachen, Germany.
E-mail address: erosadobalma@ukaachen.de (E.R. Balmayor).
[1] ORCID: 0000-0002-0484-4847.

https://doi.org/10.1016/j.ymeth.2025.06.006
Received 28 April 2025; Received in revised form 3 June 2025; Accepted 11 June 2025
Available online 11 June 2025
1046-2023/© 2025 The Author(s). Published by Elsevier Inc. This is an open access article under the CC BY license (http://creativecommons.org/licenses/by/4.0/).

populations. Following the same methodology, we also provide instructions for researchers interested in delving deeper into the endocytosis pathway —whether clathrin-mediated, caveolae-mediated, or macropinocytosis—undertaken by the delivery system, extending beyond cellular uptake evaluation. The endocytic pathway plays a pivotal role in determining the fate of internalized mRNA complexes and provides information useful in the design of more effective delivery systems [5]. Second, we describe qualitative assessment using correlative light and electron microscopy (CLEM), a powerful imaging technique that integrates fluorescence microscopy with high-resolution electron microscopy to provide spatial and structural insights into mRNA localization within cells [6]. Both methods rely on fluorescent labeling of mRNA, and we provide a detailed overview of a labeling strategy to ensure reliable tracking.

Finally, the present publication also outlines a protocol for assessing mRNA transfer to lysosomes. Investigating the mechanisms governing mRNA intracellular trafficking is critical to optimizing delivery systems. The successful internalization of mRNA complexes does not guarantee mRNA translation. Often, these complexes remain trapped in lysosomes after endocytosis, impeding cytoplasmic release [7]. Lysosomal entrapment represents a significant bottleneck in mRNA delivery, as failure to escape this degradative compartment prevents translation and diminishes therapeutic efficacy [8].

All three methods described — mRNA uptake quantification, CLEM, and lysosome trafficking — were investigated using primary human cells of translational relevance (i.e., mesenchymal stromal cells, fibroblasts, and osteoblasts), which more closely mimic physiological conditions compared to immortalized or cancer cell lines that often exhibit higher transfection efficiencies. This approach provides more accurate insights into cellular responses. Moreover, since these primary cells are extensively used in tissue engineering and regenerative medicine, studying their transfection behavior may contribute to the development and refinement of personalized therapeutic strategies for various clinical applications.

2. Materials and methods

All procedures were performed at room temperature unless otherwise specified. All chemicals, including endocytic inhibitors and heat-inactivated Fetal Bovine Serum (FBS), were purchased from Sigma-Aldrich (St. Louis, MO, USA) except otherwise indicated.

2.1. Fluorescent labeling of mRNA

mRNA used in the study, i.e., *Metridia* Luciferase (MetLuc) mRNA, was produced by *in vitro* transcription (IVT), including chemical modifications performed to improve its stability and biocompatibility with cells. IVT protocols, including purification and characterization of obtained chemically modified mRNA, have been reported by us elsewhere [9,10]. Of note, chemical modifications performed consisted of replacing 25 % of uridine residues with 2-thio-uridine, and 25 % of cytidine residues with 5-methyl-cytidine [10,11]. The mRNA integrity of all IVT-synthesized constructs was assessed using agarose gel electrophoresis and Nanodrop absorbance measurements before use. The sequence of the MetLuc mRNA used in this study can be found in the Dataverse repository (https://doi.org/10.34894/2OXOYD). In addition, representative results of the integrity assessment of the MetLuc mRNA can be found in the Dataverse repository link.

For fluorescent labeling of mRNA, we used the Label IT® Nucleic Acid Labeling Kit (MFP488, Excitation/Emission 501/523 nm, Mirus Bio, Madison, WI, USA), achieving positive results. The MFP488 Label IT® reagent was supplied as a lyophilized pellet and reconstituted prior to use. Briefly, both the reagent pellet and the reconstitution solution were brought to room temperature. For initial preparation, 100 μL of the reconstitution solution was added to each 100 μg kit pellet, followed by vortexing and brief centrifugation. The labeling reaction was assembled by sequentially adding DNase- and RNase-free water, 10 × Labeling Buffer A, the mRNA sample, and the reconstituted Label IT® reagent, following the volumes outlined in Table 1. The reaction mixture was incubated at 37 °C for 1 h, with a brief centrifugation at the 30-minute mark to minimize evaporation.

Samples were purified using G50 Microspin purification columns as recommended by the kit, although ammonium acetate precipitation was preferred for higher mRNA yields. Cold ammonium acetate (stock at 5 M) was added to the sample to a final concentration of 2.5 M, followed by incubation on ice for 30 min. The samples were then centrifuged at 20,000 g for 20 min at 4 °C, washed three times with 70 % ethanol, and centrifuged again at 20,000 g for 3 min at 4 °C. The pellet was allowed to dry and either stored at −80 °C or reconstituted with nuclease-free water. Post-labelling integrity assessment was performed (more information can be found in the Dataverse repository link). Labelling density (pmol dye/μg nucleic acid) and the base-to-dye ratio were calculated according to the manufacturer's instructions (see Table 2).

2.2. Complexation of mRNA for cellular internalization

Lipoplexes were freshly prepared in non-supplemented Opti-MEM (Life Technologies, Carlsbad, CA, USA) by mixing the selected delivery vector with labeled or unlabeled mRNA. For our studies, we used lipid-based vectors, including Lipofectamine 3000 (Invitrogen, Waltham, MA, USA) and 3DFect (OzBiosciences, Marseille, France), at an mRNA-to-vector ratio of 1:2. Volume-to-weight ratios were applied according to the manufacturers' instructions. The mRNA solution was added dropwise to the vector solution, followed by incubation for 20 min at room temperature to allow complex assembly.

Relevant to understanding cellular internalization of formed lipoplexes is to know their size and charge. Hence, dynamic light scattering (DLS; Zetasizer from Malvern Panalytical Ltd, Malvern, UK) was used to determine the size, polydispersity index (PdI), and Zeta potential of the formed lipoplexes. For these measurements, 800 μL of the MetLuc cmRNA–lipid complex, prepared in serum-free Opti-MEM, was analyzed at a fixed backscattering angle of 173°. Electrophoretic measurements were conducted using DTS1070 disposable cuvettes (Malvern Panalytical Ltd), and all determinations were performed in triplicate. The results are reported as mean hydrated particle diameter in nanometers (nm) and zeta potential in millivolts (mV).

Encapsulation efficiency of the lipoplexes was determined using the QuantiFluor® RNA System (Promega, Madison, WI, USA). Standard curves were generated using RNA solutions of known concentrations, following the manufacturer's protocol. In parallel, 1 mL of lipoplexes was prepared. For the assay, 10 μL of each complex or RNA standard was added to a 96-well plate containing the RNA-binding dye. The samples were mixed thoroughly and incubated for 5 min at room temperature, protected from light. Fluorescence was then measured using a CLARIOstar plate reader (BMG Labtech, Ortenberg, Germany) with excitation at 492 nm and emission at 540 nm. The percentage of encapsulated RNA was calculated using the following equation:

$$\textit{Encapsulation efficiency}\ (\%) = 100 - \frac{\textit{Measured nucleic acid concentration} \times 100}{\textit{Initial nucleic acid concentration}}$$

Additionally, the morphology of the lipid complexes was assessed via

Table 1
Standard Nucleic Acid Labeling Reaction.

Component	Volume
DNase-, RNase-free (molecular biology-grade) water	35 μl
10X Labeling Buffer A	5 μl
1 mg/ml nucleic acid sample	5 μl
Label IT® Reagent	5 μl
Total Volume	**50 μl**

Table 2
Labelling density of MFP488-MetLuc mRNA. Information extracted from Del Toro et al. [11] with permission from the American Society of Gene and Cell Therapy.

Sample	MFP488-MetLuc mRNA
A_{260}	0.126
A_{dye}	0.002
$C.F._{260}$	0.1
ε_{dye}	90,000
ε_{base}	8,250
A_{base}	0.1
Base: Dye ratio	**545.4**
pmol dye/µg nucleic acid	**44.09**

A260: Spectrophotometer readings (at 260 nm); **A_{dye}:** Maximum absorbance wavelength for MFP488 (A_{501}); **$C.F._{260}$:** Constant value determined by dividing the absorbance of the free dye at 260 nm with that at A_{dye}; **ε_{dye}:** Extinction coefficient of nucleic acid bound dye; **ε_{base}:** Extinction coefficient of nucleic acid.

transmission electron microscopy (TEM). A 5 µL aliquot of each sample was applied to a 300-mesh copper grid coated with a carbon film, allowed to air-dry overnight, and subsequently imaged using a Tecnai G2 Spirit BioTWIN iCorr TEM (FEI, Hillsboro, OR).

2.3. Cells and cell culture

Three different primary human cell types were used in this study: human mesenchymal stem cells (hMSCs), human dermal fibroblasts (hDFs), and human osteoblasts (hOBs). hMSCs used in this study were self-isolated. Hence, an ethical statement and brief description are provided hereafter. Following ethical approval from the ethical committee of the Maastricht University Medical Center, MUMC+, Maastricht, the Netherlands, and with written informed donor consent, bone marrow was obtained from the iliac crest of a 17-year-old, male patient. All procedures were carried out in accordance with the declaration of Helsinki in its latest amendment. hMSCs were isolated and sub-cultured as previously described [12]. In short, aspirate was resuspended using a 20-gauge needle and centrifuged to concentrate the nucleated cell portion. Thereafter, the nucleated cells were counted and plated at a density of 500,000 cells/cm^2. hMSCs were cultured in a-minimal essential medium (α-MEM; Life Technologies) with GlutaMAX supplemented with 10 % heat-inactivated fetal bovine serum (FBS) (Sigma-Aldrich) and 1 % penicillin/streptomycin (PS) (100 U/mL, Thermo Fisher Scientific, Waltham, MA). As part of a rutine quality control, isolated cells were characterized for the presence of stem cell surface markers and their ability to proliferate and differentiate as described before [12]. hDFs and hOBs were purchased from Lonza (Basel, Switzerland). hDFs were cultured in Dulbecco's modified Eagle medium (DMEM) (Thermo Fisher Scientific) supplemented with 10 % FBS and 1 % PS. hOBs were maintained in DMEM/Nutrient Mixture F-12 (1:1) (Thermo Fisher Scientific) with GlutaMAX, supplemented with 10 % FBS, 1 % PS, and 50 µg/mL ascorbic acid. All cell cultures were maintained in a humidified atmosphere at 37 °C with 5 % CO_2.

2.4. mRNA transfer into cells

Depending on the assay, cells were seeded in different well plate formats 24 h before transfection (see Table 3) to ensure a sufficient cell number for analysis. In this study, hMSCs, hDFs, or hOBs were seeded at a density of 15,000 cells/cm^2. After 24 h, the culture medium was removed from the wells, and freshly prepared mRNA complexes were added for transfection. Further details on the transfection procedures for each assay are provided in the following sections.

Table 3
Summary of transfection conditions for the various assays described.

Assays	Plate format	Volume per well
Flow cytometry – Endocytosis pathway determination	24-wells	500 µl
CLEM – Cellular uptake of mRNA complexes	8-wells Ibidi µ-Slide	300 µl
Luminescent measurements – Transfection efficiency	96-wells White opaque plate	100 µl
Microscopy – Trafficking of internalized mRNA complexes	96-wells Glass bottom plate	100 µl

2.5. Transfection efficiency

At 1-, 2-, and 3-days post-transfection, supernatants from hMSCs, hDFs, and hOBs transfected with MetLuc cmRNA were collected and stored at –80 °C for subsequent analysis of MetLuc activity. For quantification, 50 µL of native coelenterazine (50 µM in degassed sodium phosphate buffer, pH 7.0; Synchem, Felsberg, Germany) was added to 50 µL of cell supernatant in a white opaque 96-well plate. Luminescence was immediately measured at 480 nm using a CLARIOSTAR plate reader (BMG Labtech) and expressed as relative light units (RLU) at room temperature. Each group consisted of n = 3 biological replicates.

2.6. Quantification of mRNA uptake using flow cytometry

Flow cytometry was used to quantify the cellular uptake of mRNA complexes and identify the specific endocytic mechanisms responsible for their internalization. Twenty-four hours before transfection, cells (i.e., hMSCs, hDFs, or hOBs) were seeded in 24-well plates at a density of 15,000 cells/cm^2. After 24 h, cells were pre-incubated with the endocytic inhibitors chlorpromazine, wortmannin, or genistein in non-supplemented Opti-MEM (Life Technologies) for one hour before transfection. Since the effects of these inhibitors are dose-dependent and may vary between cell types [8], it is essential to assess their cytotoxicity to determine the optimal concentration for uptake experiments. Cytotoxicity can be evaluated using assays such as the PrestoBlue™ Cell Viability Reagent (Invitrogen) or the MTS Assay Kit (Abcam, Cambridge, UK), among others. The tested concentration ranges for each inhibitor and the final selected concentrations are summarized in Table 4.

For the experiments, labeled and unlabeled mRNA complexes were freshly prepared in Opti-MEM. These complexes were then added to a non-supplemented Opti-MEM solution containing the selected inhibitor at the appropriate concentration. Cells were incubated with the mRNA complex solution for one hour. Following incubation, the medium containing the complexes was removed, and cells were washed three

Table 4
Range of concentrations for each endocytic inhibitor. The selected concentrations are depicted in bold. Concentrations higher than those indicated (bold) may increase cytotoxicity. Although this effect is dependent on the cell type. Of note, genistein is particularly toxic for hDFs. Hence, concentrations > 200 µM should be avoided. More details on the cytotoxicity of these inhibitors with increasing concentrations can be found elsewhere [11]. Information extracted from Del Toro et al. [11] with permission from the American Society of Gene and Cell Therapy.

Chlorpromazine (µM)	Wortmannin (µM)	Genistein (µM)
5.6	0.01	100
11.3	0.02	150
16.9	0.03	**200**
22.5	0.04	250
28.1	**0.05**	300
33.8	0.06	350
39.4	0.07	400

times with PBS (Gibco, Waltham, MA, USA).

Cells were detached using 0.05 % trypsin (Gibco), centrifuged at 500 g for five minutes, and the trypsin was removed. The cell pellets were resuspended in ice-cold PBS and kept on ice until analysis. Flow cytometry was performed using a BD Accuri C6 Plus Flow Cytometer (BD Biosciences, Franklin Lakes, NJ, USA). Forward and side scatter density plots were used to identify the cell population, and 5,000 events were collected per sample. It must be ensured that the flow cytometer is equipped with the appropriate filters for detecting the dye selected in Section 2.1. The percentage of fluorescent-positive cells was calculated using FlowJo Software v.10 (BD Biosciences).

2.7. Visualization of labelled mRNA using CLEM

An excellent technique to visualize the internalization of labeled mRNA inside cells is correlative light and electron microscopy, also known as CLEM. This technique combines fluorescence microscopy with high-resolution electron microscopy. In our work, a confocal microscope was combined with a transmission electron microscope for this purpose. For this, cells were seeded on µ-Slide 8-well culture dishes (Ibidi, Gräfelfing, Germany) at a density of 15,000 cells/cm^2. Ibidi µ-Slides feature an imprinted coordinate system that allows the precise localization of individual and specific cells in the TEM microscope after the desired region of interest is imaged with confocal microscopy (see Fig. 1). After 24 h, cells were transfected with labeled mRNA complexes and incubated for 1 h, followed by three washes with PBS. Samples were fixed with 1.6 % glutaraldehyde in PBS for 20 min at room temperature and washed twice with PBS. Cell nuclei were stained with Hoechst 34,580 (Thermo Fisher Scientific), washed twice with PBS, and actin filaments were stained with Phalloidin Alexa Fluor® (AF647, Thermo Fisher Scientific) followed by two additional PBS washes. The selected phalloidin should have a different fluorophore from the labeled mRNA. Samples were kept in PBS for imaging purposes. An overview of the coordinate system was imaged using a 10 × objective, and a central area of the coordinate system was selected for high-resolution imaging with an 86 × water immersion objective. Pictures of all channels (nuclear staining, phalloidin, and labeled mRNA) were acquired. The confocal microscope SP8 from Leica Microsystems was used for analysis and imaging.

After confocal acquisition, the same sample was processed for TEM. PBS was removed, and samples were kept in 0.1 M cacodylic acid sodium salt trihydrate (cacodylate buffer, Thermo Fisher Scientific) at 4 °C for 24 h. Samples were washed three times for 15 min each with 0.1 M cacodylate buffer, incubated in a buffer containing 1 % osmium tetroxide (Electron Microscopy Sciences, EMS, Hatfield, PA, USA) and 1.5 % potassium ferricyanide ($K_3[Fe(CN)_6]$) protected from light at 4 °C for 1 h. Subsequently, a dehydration process was performed. For this, samples were immersed in a graded series of ethanol washes (70 %–90 %–100 %) for 30 min. Incubation in each ethanol solution was repeated twice. Samples were infiltrated with Epon resin (LADD Research, Williston, VT, USA) for two days, followed by a two-days polymerization at 60 °C. Epon blocks were trimmed using an ultramicrotome (Leica Microsystems, Wetzlar, Germany) with a diamond trimming knife (Diatome, Hatfield, PA, USA). Cells within the region of interest (ROI) were identified and imaged using the Tecnai G2 Spirit BioTWIN TEM (FEI) operated at 120 kV and with a WA-Veleta camera (EMSIS GmbH, Münster, Germany). TEM images were overlapped with the confocal images for the exact location, e.g., same investigated cell. Specific areas of interest, for example where the labeled complexes were located, were further inspected at higher magnifications and imaged. Fiji software

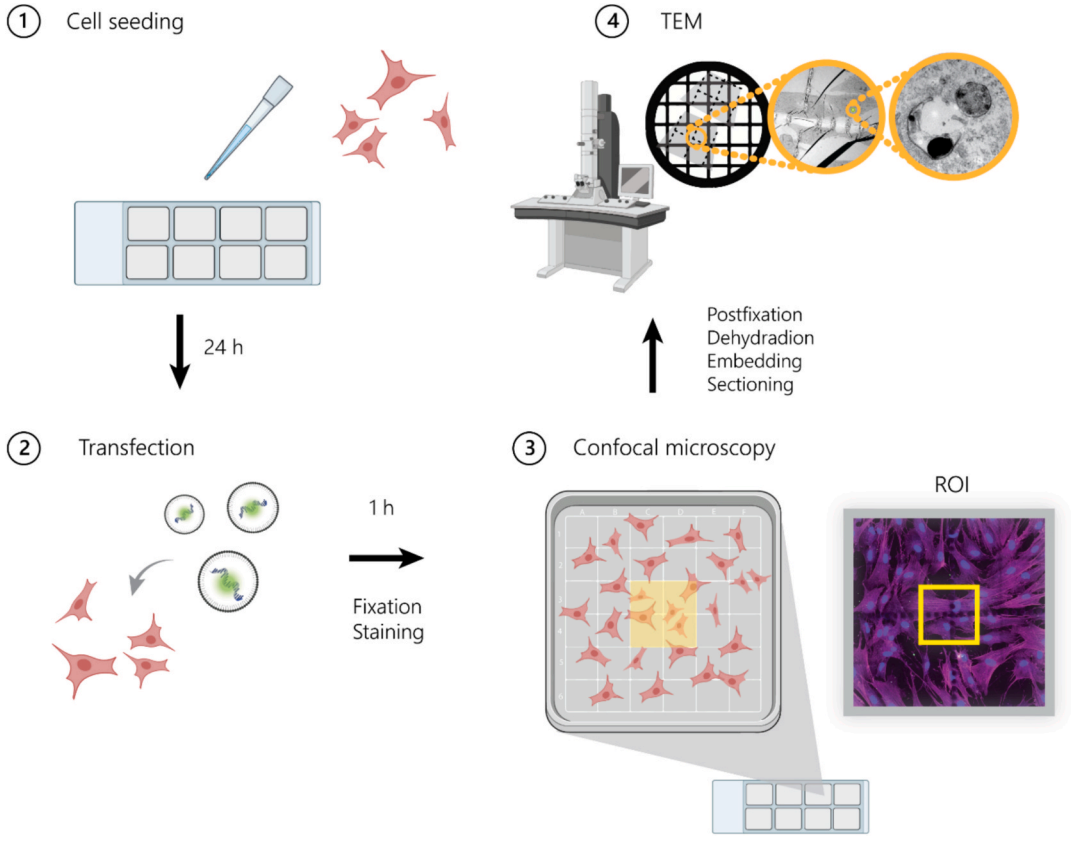

Fig. 1. Procedure for CLEM imaging. Cells are seeded on a µ-Slide 8-Well culture dishes that features a coordinate system. After 24 h, cells are transfected with MFP488-labeled mRNA. A region of interest is selected to image with high-resolution microscopy. Sample preparation for TEM includes post-fixation with buffer containing 1% osmiumtetroxide and 1.5% potassium ferricyanide ($K_3[Fe(CN)_6]$, dehydration in a graded series of ethanol, Epon resin infiltration, embedding, and sectioning. Adapted from Del Toro et al. [11] with permission from the American Society of Gene and Cell Therapy.

(https://fiji.sc/, [13]) was used for image processing. Confocal and TEM images were superimposed using the imprinted coordinate system and nuclei patterns to facilitate easy recognition of the defined ROI.

2.8. Trafficking of mRNA to lysosomes

Cells were seeded onto 96-well plates with optical bottoms suitable for microscopy using a cell suspension of 50,000 cells/ml. After 24 h, transfection complexes with labeled mRNA were prepared. LysoTracker™ Deep Red (Invitrogen) was added to the transfection solution at a concentration of 150 nM. Cells were transfected for 3 h, washed with PBS, and fixed with 4 % paraformaldehyde (PFA). The 3-hour post-transfection time point was selected based on prior live-cell imaging showing reliable visualization of mRNA trafficking to lysosomes, preceding the onset of protein expression (typically 4–6 h) [11]. Nuclear staining was performed, and images of the LysoTracker™ dye, nuclei, and labeled complexes were acquired with a high-resolution microscope to visualize possible colocalization of internalized complexes. High-resolution images were acquired with the inverted SP8 confocal microscope (Leica Microsystems) using a 100× oil immersion objective (HC PL APO 100/1.20 OIL, Leica Microsystems). Colocalization analysis was carried out using Fiji software (https://fiji.sc/, [13]); the total number of lysosomes and mRNA complexes was quantified automatically using the "Find Maxima" function, while colocalized lipoplexes were manually counted.

2.9. Statistical analysis

All the obtained values are reported as mean ± standard deviation. Statistical analysis was performed using GraphPad Prism v.8.00 (GraphPad Software, San Diego, CA, USA). Ordinary one-way or two-way ANOVA with Geisser-Greenhouse correction, followed by Dunnett's multiple comparisons test were performed to analyze multiple groups. Probabilities of $p < 0.05$ were considered significant. P-values are reported as * $p \leq 0.05$, ** $p \leq 0.01$, *** $p \leq 0.001$, and **** $p \leq 0.0001$.

3. Results

3.1. Lipoplex characterization

MetLuc cmRNA lipoplexes exhibited a mean particle size of approximately 400 nm and a polydispersity index (PdI) 0.26, indicating monodispersity within an acceptable range for nanoparticle formulations (Fig. 2**A**). Interestingly, the lipoplexes were negatively charged with a near-neutral zeta potential of –4 mV. Encapsulation efficiency was notably high with lipoplexes showing minimal unbound mRNA, suggesting nearly complete encapsulation. TEM further confirmed the structural features of the lipoplexes (Fig. 2**B**), revealing predominantly semi-spherical morphologies with internal compartments, or vesicles, typically centralized within each complex.

3.2. Transfection efficiency

Notable differences in MetLuc protein expression following inhibition of endocytic pathways were observed among the different cell types (Fig. 2**C**). Of note, chlorpromazine, wortmannin, and genistein were used to inhibit clathrin-mediated endocytosis, macropinocytosis, and

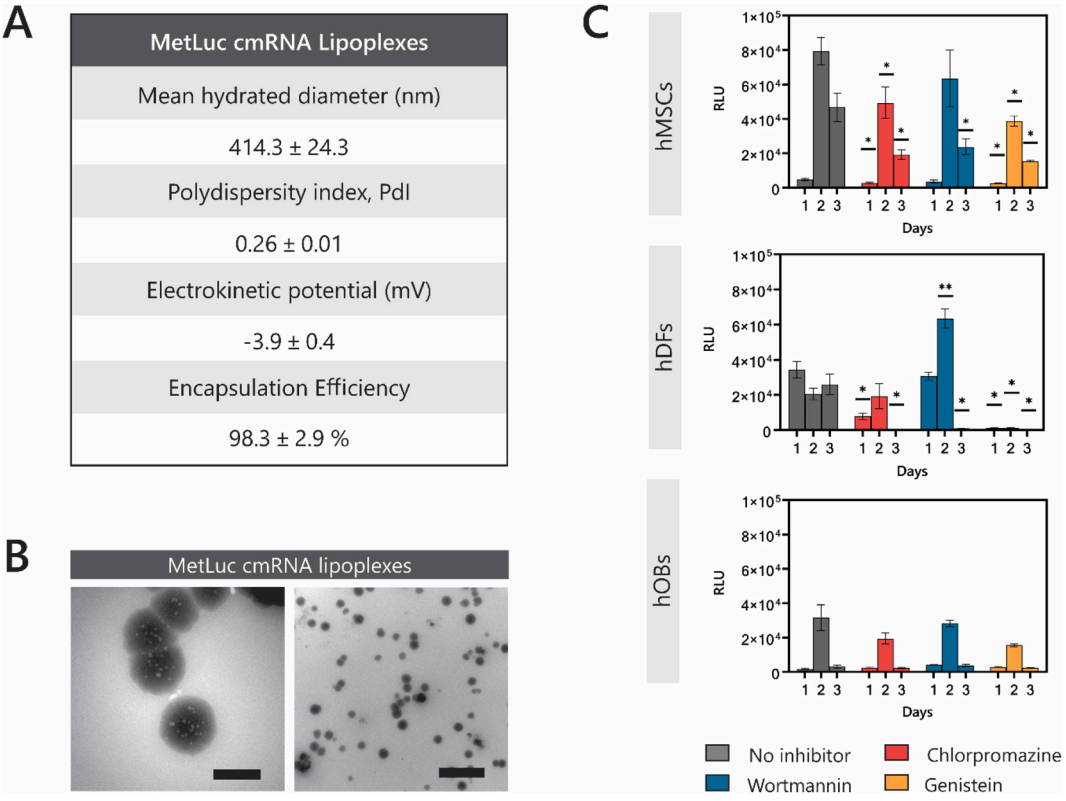

Fig. 2. Physicochemical characterization of lipoplexes and their transfection efficiencies. (A) Summary table of the main physicochemical properties of the mRNA-lipid complexes, including hydrodynamic size, polydispersity index, zeta potential, and encapsulation efficiency. (B) Transmission electron microscopy images show that the lipoplexes exhibit predominantly spherical morphologies with multiple inner vesicles. Scale bars: left image = 200 nm, right image = 1000 nm. (C) Transfection efficiencies assessed by luminescence measurements in hMSCs, hDFs, and hOBs following treatment with or without endocytosis inhibitors. Statistical analysis was performed using two-way ANOVA with Geisser-Greenhouse correction, followed by Dunnett's multiple comparisons test. * $p \leq 0.05$, ** $p < 0.01$. Abbreviations: MetLuc, Metridia luciferase; hMSCs, human mesenchymal stromal cells; hDFs, human dermal fibroblasts; hOBs, human osteoblasts; RLU, relative light units.

caveolae-mediated endocytosis, respectively. In hMSCs, treatment with chlorpromazine or genistein led to a significant reduction in MetLuc expression compared to the control group (no inhibition; $p < 0.05$). This inhibitory effect on the protein expression was persistent for all time of observation evaluated. In contrast, the inhibitory effect of wortmannin on the hMSCs protein expression was only significant at day 3 post-transfection ($p < 0.05$). Unexpectedly, in hDFs, a treatment with wortmannin resulted in a significant increase in MetLuc expression two days after mRNA transfection ($p = 0.0018$ compared to control). Conversely, genistein caused a marked, significant reduction in protein secretion levels for all times of observation evaluated ($p < 0.05$ compared to control). Interestingly, in hOBs, inhibition of endocytic pathways with any of the three compounds did not result in significant changes in MetLuc expression, suggesting a distinct uptake or processing mechanism for this cell type.

3.3. Quantification of mRNA uptake using flow cytometry

Using chlorpromazine, wortmannin, and genistein, the mechanisms of endocytosis of MFP488-labeled mRNA lipoplexes were investigated. The percentage of cellular mRNA uptake, before and after endocytosis inhibition, was determined using flow cytometry, with untransfected cells used as a negative control.

The uptake of mRNA by hMSCs and its quantification are shown in Fig. 3**A-F**. In the absence of inhibitors, 30.7 ± 9.5 % of the lipoplexes was internalized by hMSCs (Fig. 3**A and 3C**). While wortmannin showed no significant effect on mRNA uptake (Fig. 3**A and E**, reduction to 24.1 ± 3.1 %, n.s., $p = 0.2844$), chlorpromazine and genistein treatments significantly blocked mRNA uptake to near 0 % values (Fig. 3**D and 3F**, uptake < 1.96 %, $p < 0.0001$).

A similar mRNA uptake pattern was observed in hDFs (Fig. 4**A-F**). Also, for this cell type, a treatment with wortmannin did not show a significant effect on mRNA uptake compared to transfected cells without inhibition (Fig. 4**A and 4E**, uptake = 32.6 ± 12.4 %, $p = 0.4132$). On the contrary, genistein treatment (Fig. 4**A and 4F**) caused the most pronounced reduction in cellular uptake, lowering it to 1 ± 0.091 % ($p < 0.0001$), followed by chlorpromazine (Fig. 4**A and 4D**), which reduced uptake to 17.6 ± 1.01 % ($p = 0.0052$).

In line with previous results in hMSCs and hDFs, wortmannin treatment did not influence the mRNA uptake by the hOBs (Fig. 5**A-F**, uptake = 19.7 ± 6.2 % upon wortmannin vs. 20.7 ± 7.75 % without inhibition, $p = 0.9961$). However, both chlorpromazine (Fig. 5**A and 5D**) and genistein (Fig. 5**A and 5F**) treatments significantly decreased mRNA uptake to 7.8 ± 0.7 % and 7.5 ± 1.9 %, respectively, compared to the transfected group with no inhibitors (Fig. 5**C**, $p = 0.0209$ and $p = 0.0180$, respectively).

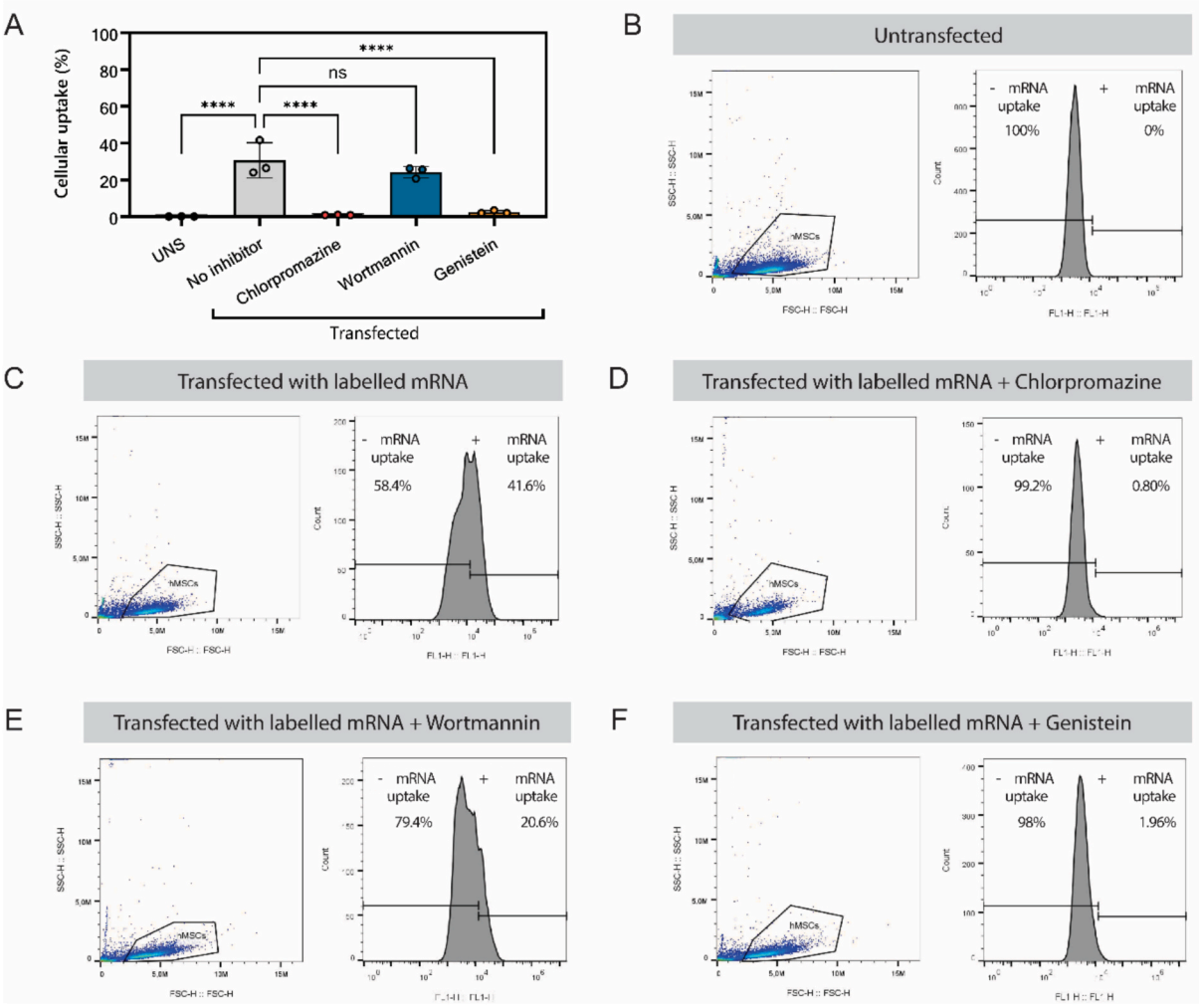

Fig. 3. Quantification of MFP488-labeled MetLuc lipoplex uptake in hMSCs using flow cytometry. (A) Summary of quantification results presented as mean ± SD (n = 3). (B) Untransfected hMSCs serving as a negative control. (C) Transfected hMSCs without inhibitors. Transfected hMSCs treated with (D) chlorpromazine, (E) wortmannin, or (F) genistein to inhibit clathrin-mediated endocytosis, macropinocytosis, or caveolae-mediated endocytosis, respectively. Percentages displayed in panels B–F represent replicated data. Statistical analysis was performed using one-way ANOVA followed by Dunnett's multiple comparison test. **** $p < 0.0001$. MetLuc, Metridia luciferase; hMSCs, human mesenchymal stromal cells.

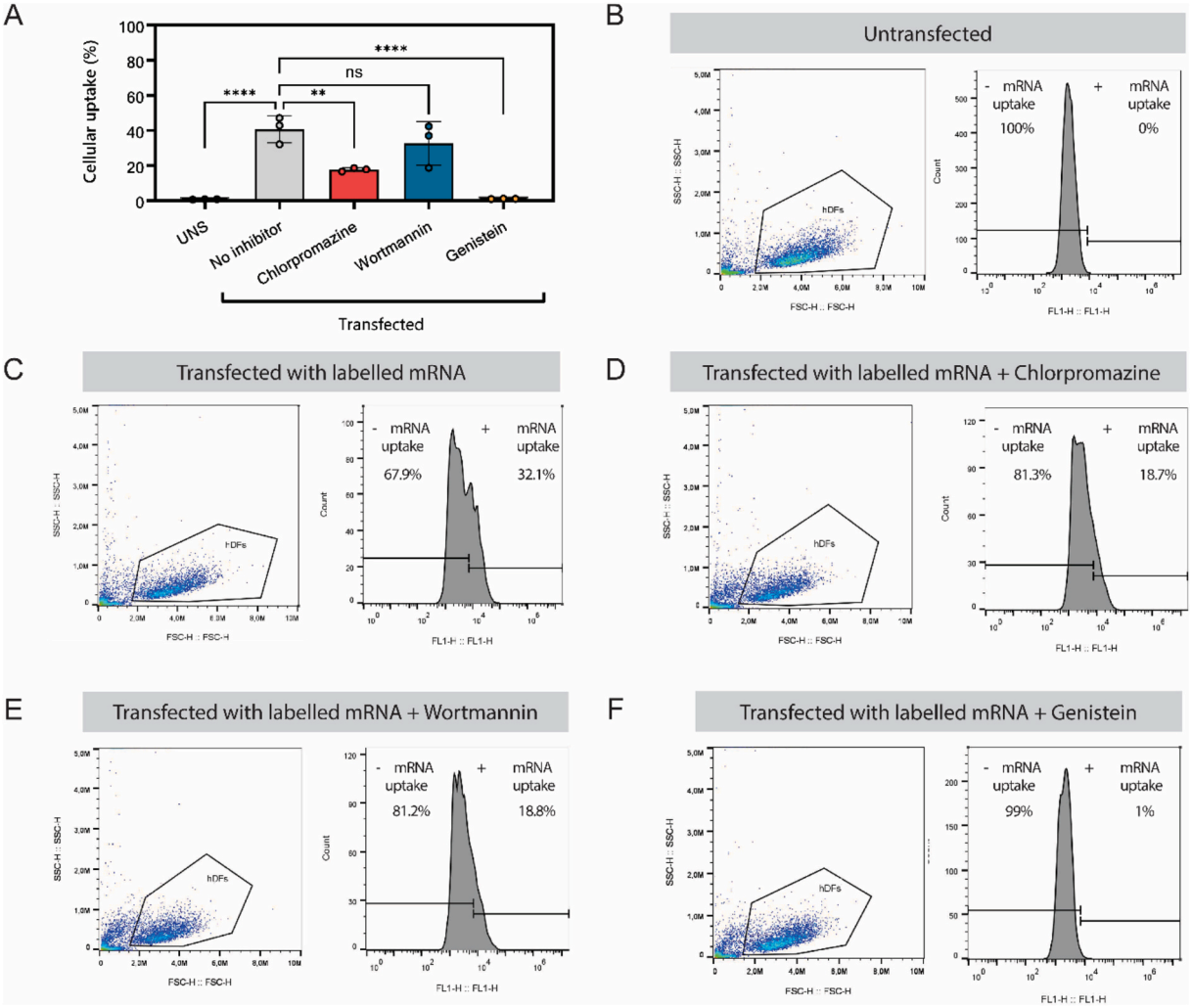

Fig. 4. Quantification of MFP488-labeled MetLuc lipoplex uptake in hDFs using flow cytometry. (A) Summary of quantification results presented as mean ± SD (n = 3). (B) Untransfected hDFs serving as a negative control. (C) Transfected hDFs without inhibitors. Transfected hDFs treated with (D) chlorpromazine, (E) wortmannin, or (F) genistein to inhibit clathrin-mediated endocytosis, macropinocytosis, or caveolae-mediated endocytosis, respectively. Percentages displayed in panels B–F represent replicate data. Statistical analysis was performed using one-way ANOVA followed by Dunnett's multiple comparison test. **p < 0.01, **** p < 0.0001. MetLuc, Metridia luciferase; hDFs, human dermal fibroblasts.

3.4. Visualization of labelled mRNA using CLEM

Fluorescent images were overlaid with transmission electron photomicrographs of the same cells to visualize the cellular uptake of mRNA lipid complexes. ROIs selected for analysis are shown for hMSCs (Fig. 6**A**), hDFs (Fig. 6**B**), and hOBs (Fig. 6**C**). Cell nuclei are depicted in blue, actin filaments are stained magenta, and MFP488-labeled lipoplexes are visible as green dots. At 1 h post-transfection, some lipoplexes appeared to initiate internalization through cell membrane invaginations (Fig. 6**Aiii**). Additionally, lipoplexes were observed near the cell membrane (e.g., Fig. 6**Biv and 6Bvi**) or internalized within the cytosol, often in proximity to the nucleus, where they appeared to be enclosed in endosomes or undergoing degradation (e.g., Fig. 6**Aiii and 6Av**). In hOBs, certain lipoplexes remained bound to the cell membrane (Fig. 6**Civ and 6Cv**), exhibiting association with caveolae-like structures.

3.5. Trafficking of mRNA to lysosomes

To further investigate the intracellular trafficking of mRNA complexes after internalization, acidic lysosomes were visualized with a red punctate staining pattern, MFP488-labeled complexes appeared in green, and cell nuclei were stained blue (Fig. 7**A-C**). At 3 h post-transfection, lipoplexes were detected in three distinct locations: the cytosol, the extracellular space, and colocalized with lysosomes. High-resolution confocal microscopy confirmed colocalization, indicated by yellow signals resulting from the overlap of red lysosomal staining and green fluorescence from the complexes. Representative regions of colocalization are highlighted within the dotted boxes (Fig. 7**A-C**). While most complexes remained in the cytosol, a smaller portion was found within lysosomes (Fig. 7**D**). Interestingly, hOBs accumulated mRNA lipoplexes in lysosomes, twice as many as the hMSCs, however, overall percentages of trafficking to lysosomes ranged from 2-4 % (Fig. 7**E**).

4. Discussion and conclusions

The development of mRNA-based therapeutics has seen a fast-paced growth in recent years, largely due to their ability to provide rapid and adaptable solutions to public health needs [14]. However, the therapeutic success of mRNA relies not only on its coding capacity but also critically on its effective delivery to the cytosol, where it can be translated into functional proteins [15].

Understanding the extent of mRNA uptake and its intracellular

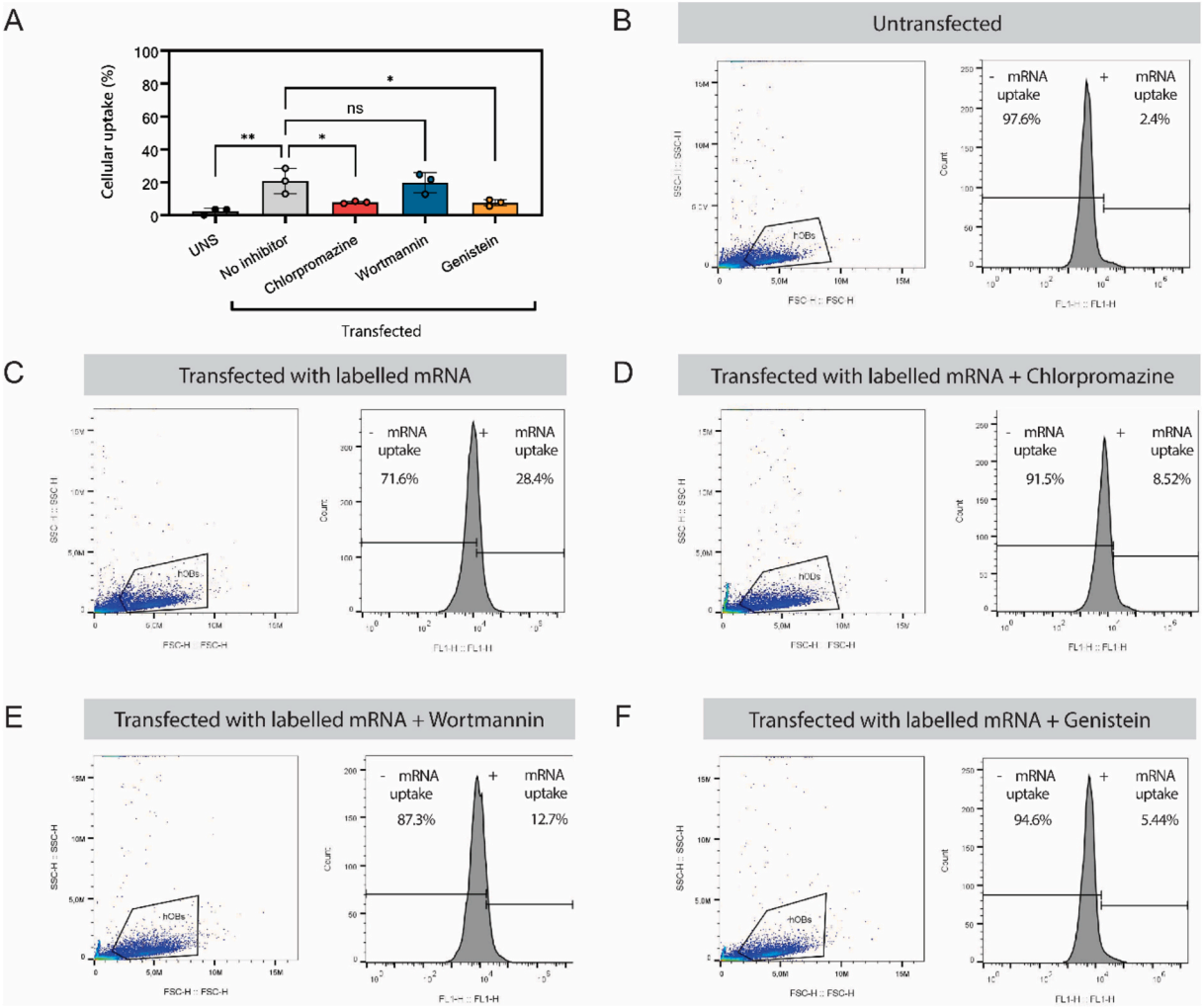

Fig. 5. Quantification of MFP488-labeled MetLuc lipoplex uptake in hOBs using flow cytometry. (A) Summary of quantification results presented as mean ± SD (n = 3). (B) Untransfected hOBs serving as a negative control. (C) Transfected hOBs without inhibitors. Transfected hOBs treated with (D) chlorpromazine, (E) wortmannin, or (F) genistein to inhibit clathrin-mediated endocytosis, macropinocytosis, or caveolae-mediated endocytosis, respectively. Percentages displayed in panels B–F represent replicate data. Statistical analysis was performed using one-way ANOVA followed by Dunnett's multiple comparison test. * $p < 0.05$, ** $p < 0.01$. MetLuc, Metridia luciferase; hDFs, human dermal fibroblasts.

trafficking helps determine whether the delivery system is effective in overcoming the extracellular and intracellular barriers. This knowledge is essential for the optimal design of effective nonviral gene-delivery carriers [16]. Various approaches can be employed to study the internalization and post endocytic trafficking of gene carrier complexes. In this methodological paper, we demonstrated the feasibility of fluorescently labeling mRNA and quantitatively evaluating cellular uptake percentages with and without the influence of different endocytic pathway inhibitors. This method offers the advantage of being relatively easy to use, allowing for the quantitative description of cellular uptake in large cell populations and facilitating the study of multiple conditions.

This study investigated three major endocytic pathways—clathrin-mediated endocytosis, caveolae-mediated endocytosis, and macropinocytosis—using specific inhibitors for each pathway. Understanding these pathways is crucial because the endocytic mechanism dictates how mRNA complexes are trafficked within the cell, their eventual fate (e.g., degradation in lysosomes, or successful trafficking to the cytoplasm for translation) [17].

We found that chlorpromazine and genistein, inhibitors of clathrin-mediated and caveolae-mediated endocytosis, respectively, significantly reduced mRNA uptake in human primary cells. This highlights the importance of these pathways in mRNA internalization. Conversely, wortmannin, which targets macropinocytosis, did not show a significant reduction in mRNA uptake, suggesting that macropinocytosis plays a minor or cell-type-specific role in this context. These findings align with previous reports indicating that clathrin- and caveolae-mediated mechanisms are the predominant routes for internalizing mRNA-containing nanoparticles [11,18].

Notably, our lipoplexes exhibited an average hydrodynamic diameter of ~ 400 nm, a size range that, according to Rejman et al., favors internalization via clathrin- or caveolae-mediated pathways, with caveolae-mediated uptake becoming increasingly dominant as particle size increases beyond ~ 200 nm [19]. This is consistent with our findings, where inhibition of caveolae and clathrin-mediated uptake significantly impacted mRNA internalization. Additionally, the near-zero zeta potential (~ –4 mV) of our particles is of particular relevance. While positively charged nanoparticles are commonly used to enhance electrostatic interactions with the negatively charged cell membrane, they can also lead to increased cytotoxicity, rapid clearance, and non-specific interactions [20]. In contrast, mildly negative or neutral nanoparticles, such as those used in this study, typically demonstrate enhanced biocompatibility and reduced serum protein adsorption, though they may rely more heavily on receptor-mediated

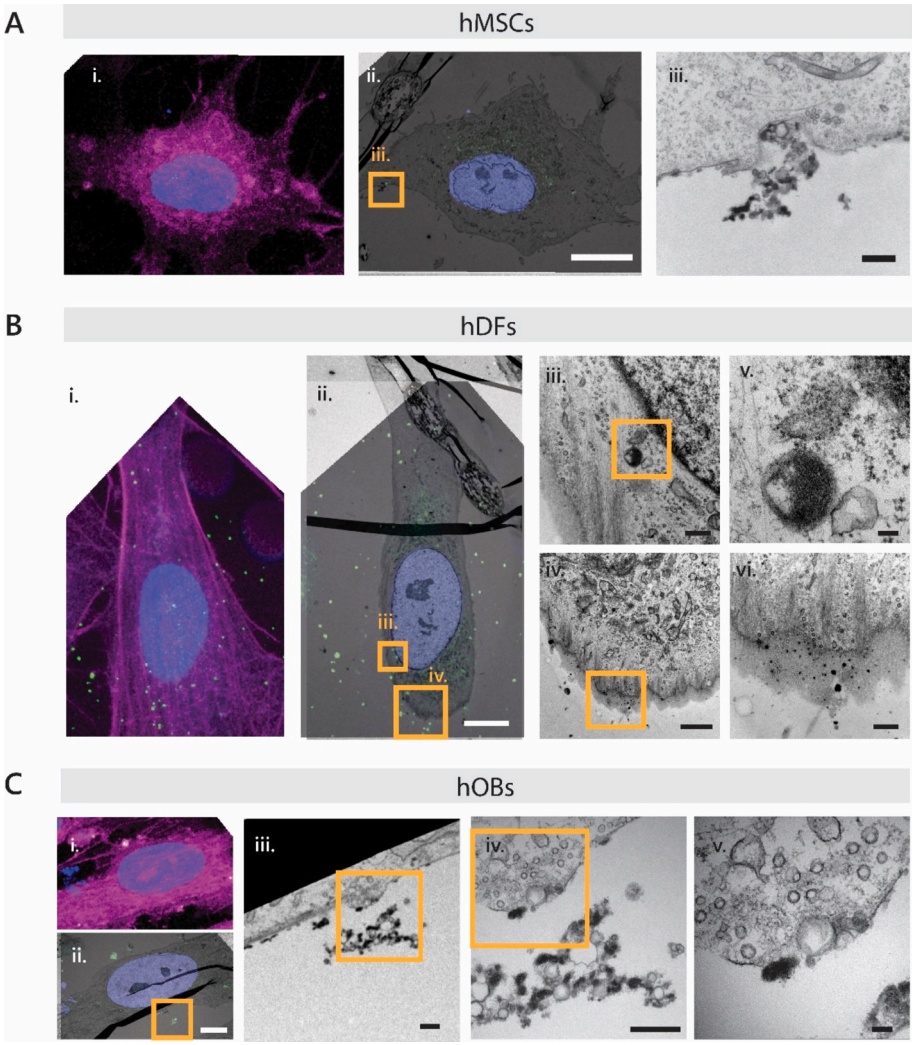

Fig. 6. CLEM of cells upon transfection with MFP 488 labeled mRNA lipoplexes. (A) hMSCs, (B) hDFs, and (C) hOBs. (i) Nuclear staining with Hoechst is shown in blue, actin filaments stained with phalloidin in magenta, and MFP 488 labelled lipoplexes are in green. (ii) Correlated confocal and TEM images of the same cell. (iii-vi) are sections representing high magnified regions of interest framed in yellow in the correlated image. Scale bars in (ii) 10 μm, in (iii and vi) 500 nm, in (iv) and 2 μm and in (v) 100 nm. CLEM, correlative light and electron microcopy; hMSCs, human mesenchymal stromal cells; hDFs, human dermal fibroblasts; hOBs, human osteoblasts. (For interpretation of the references to colour in this figure legend, the reader is referred to the web version of this article.)

uptake mechanisms rather than non-specific electrostatic interactions [21]. Although flow cytometry is an effective tool for mRNA quantification, it may have limitations in terms of providing spatial and structural information about mRNA localization within cells. This limitation can be addressed by combining flow cytometry with other imaging techniques, such as CLEM for more comprehensive analysis. We qualitatively assessed the internalization of fluorescent mRNA complexes using this technique, which allowed us to identify internalized lipoplexes in the cytosol, or right in the process of internalization forming invaginations with the cell membrane and caveolae-like structures. These visual representations offer a complementary information to flow cytometry data.

Transfection efficiency results highlighted the cell-type specific dependency on endocytic routes. In hMSCs and hDFs, treatment with chlorpromazine or genistein significantly reduced MetLuc protein expression, indicating that both clathrin- and caveolae-mediated endocytosis are key routes for the internalization and functional delivery of mRNA lipoplexes. Notably, in hDFs, inhibition of caveolae-mediated uptake led to an almost complete loss of protein expression. This suggests that although both pathways contribute to lipoplex internalization, caveolae-mediated endocytosis may also play a more critical role in promoting efficient endosomal escape and cytosolic release, making it particularly essential for productive transfection in hDFs.

In contrast, hOBs transfection efficiency appeared largely unaffected by any of the inhibitors, implying that either alternative internalization pathways or compensatory mechanisms are predominant in this cell type. One possible mechanism is phagocytosis. While traditionally associated with specific cell types such as macrophages, dendritic cells, and osteoclasts, previous studies have reported that osteoblasts are also capable of internalizing particles through phagocytic-like processes [22].

To further evaluate the intracellular trafficking and destination of mRNA complexes, we provided a protocol to visually determine entrapment in lysosomal compartments. By overlapping fluorescence channels corresponding to lysosomal markers and labeled mRNA, we determined whether mRNA complexes were predominantly entrapped in lysosomes, partially colocalized, or successfully bypassed degradative compartments. Such insights are vital, as lysosomal entrapment directly correlates with reduced cytosolic release and diminished protein production [23]. Our study showed that, while some mRNA complexes were successfully internalized into the cytosol, a portion remained entrapped in lysosomes, indicating that delivery vectors can be further improved to enhance efficient endosomal escape and cytosolic release of the mRNA cargo. A comparable strategy was reported by Dirisala et al., who

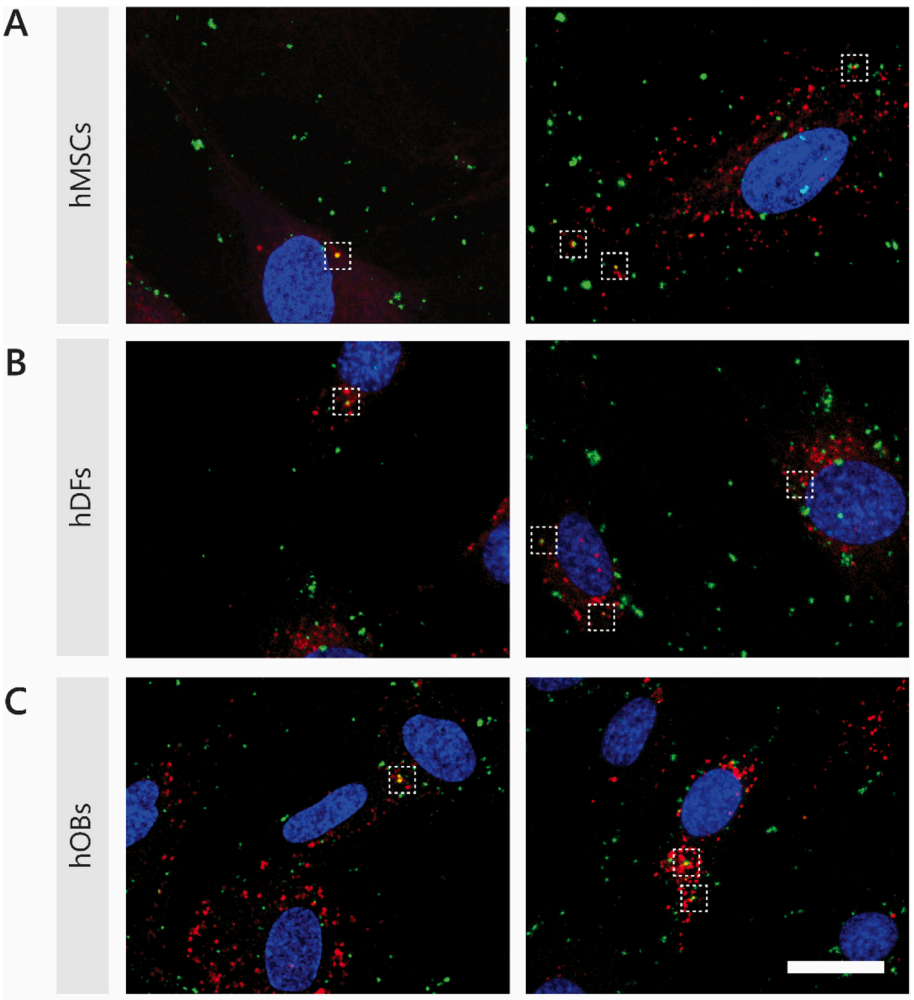

D

Cell	Colocalized mRNA	Total mRNA	Total lysosomes
hMSCs	9 ± 1.7	364 ± 100	671 ± 222
hDFs	11 ± 2.0	566 ± 107	735 ± 173
hOBs	18 ± 9.0	479 ± 89	710 ± 66

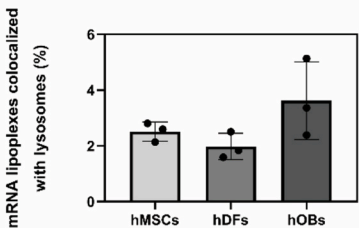

Fig. 7. Lysosome trafficking of cells transfected with MFP-488 labelled mRNA lipoplexes. (A) hMSCs, (B) hDFs, and (C) hOBs. Images were acquired 3 h post-transfection. LysoTracker™ Deep Red-stained acidic compartments in red, nuclear staining with Hoechst is shown in blue and MFP-488 labelled complexes in green. Dashed squares indicate ROIs with colocalized complexes and lysosomes. (**D**) and (**E**) Quantification of colocalized lipoplexes with lysosomes. Scale bar: 20 μm. hMSCs, human mesenchymal stromal cells; hDFs, human dermal fibroblasts; hOBs, human osteoblasts. (For interpretation of the references to colour in this figure legend, the reader is referred to the web version of this article.)

demonstrated that wrapping ternary polyplexes with a pH-responsive, charge-conversion polymer significantly improved endosomal escape of Cy5-labeled mRNA in human umbilical vein endothelial cells (HUVECs), resulting in up to an 80-fold increase in protein expression compared to polyplexes lacking the responsive element [24]. Studies in the context of lysosome trafficking may benefit from adding drugs that either enhance or inhibit endosome release, i.e., chloroquine or bafilomycin, respectively [25]. Chloroquine is a lysosomotropic agent that promotes rupture of endosomes through protonation in an acidic environment [25], while bafilomycin, an inhibitor of vacuolar-type-H^+-ATPases, inhibits endosomal escape by resulting in the accumulation of cargo in lysosomes [26]. By using these drugs, researchers can dissect the specific mechanisms underlying the trafficking and fate of mRNA complexes. For example, if the delivery system's efficacy improves in the presence of chloroquine, it may indicate that endosomal trapping was a bottleneck in the transfection process. Moreover, ongoing advancements in imaging technologies, such as live-cell imaging and super-resolution microscopy, may allow for real-time tracking of mRNA complexes within cells, providing even more detailed insights into their intracellular behavior [27,28].

This study highlights the importance of understanding the cellular uptake and intracellular trafficking of mRNA complexes in primary human cells. The combination of quantitative and qualitative techniques enables a comprehensive evaluation of mRNA delivery efficiency, offering valuable tools for improving the design of next-generation mRNA therapeutics.

CRediT authorship contribution statement

Claudia Del Toro Runzer: Conceptualization, Formal analysis, Investigation, Methodology, Visualization, Writing – original draft. **Christian Plank:** Funding acquisition, Resources. **Martijn van Griensven:** Conceptualization, Funding acquisition, Project administration, Supervision. **Elizabeth R. Balmayor:** Conceptualization, Funding acquisition, Supervision, Visualization, Writing – review & editing.

Declaration of competing interest

The authors declare the following financial interests/personal relationships which may be considered as potential competing interests: Christian Plank reports financial support was provided by Horizon 2020. Martijn van Griensven reports financial support was provided by Horizon 2020. Elizabeth Balmayor reports financial support was provided by Horizon 2020. Christian Plank reports a relationship with Ethris GmbH that includes: employment. Christian Plank has patent #US20180214572A1 issued to assignee. Elizabeth Balmayor has patent #US20180214572A1 issued to assignee. none If there are other authors, they declare that they have no known competing financial interests or personal relationships that could have appeared to influence the work reported in this paper.

Acknowledgement

This work has been performed as part of the cmRNAbone project funded by the European Union's Horizon 2020 research and innovation programme under the Grant Agreement No 874790.

Data availability

Data will be made available on request.

References

[1] A. Wadhwa, A. Aljabbari, A. Lokras, C. Foged, A. Thakur, Opportunities and challenges in the delivery of mRNA-based vaccines, Pharmaceutics 12 (2) (2020) 102.
[2] A. Dirisala, S. Uchida, T.A. Tockary, N. Yoshinaga, J. Li, S. Osawa, L. Gorantla, S. Fukushima, K. Osada, K. Kataoka, Precise tuning of disulphide crosslinking in mRNA polyplex micelles for optimising extracellular and intracellular nuclease tolerability, J. Drug Target. 27 (5–6) (2019) 670–680.
[3] K.A. Hajj, K.A. Whitehead, Tools for translation: non-viral materials for therapeutic mRNA delivery, Nat. Rev. Mater. 2 (10) (2017).
[4] C. Lorenz, M. Fotin-Mleczek, G. Roth, C. Becker, T.C. Dam, W.P. Verdurmen, R. Brock, J. Probst, T. Schlake, Protein expression from exogenous mRNA: uptake by receptor-mediated endocytosis and trafficking via the lysosomal pathway, RNA Biol. 8 (4) (2011) 627–636.
[5] J.E. Ziello, Y. Huang, I.S. Jovin, Cellular endocytosis and gene delivery, Mol. Med. 16 (2010) 222–229.
[6] P. De Boer, J.P. Hoogenboom, B.N. Giepmans, Correlated light and electron microscopy: ultrastructure lights up!, Nat. Methods 12 (6) (2015) 503–513.
[7] D. Pei, M. Buyanova, Overcoming endosomal entrapment in drug delivery, Bioconjug. Chem. 30 (2) (2018) 273–283.
[8] S. Chatterjee, E. Kon, P. Sharma, D. Peer, Endosomal escape: a bottleneck for LNP-mediated therapeutics, Proc. Natl. Acad. Sci. 121 (11) (2024) e2307800120.
[9] R.E. De La Vega, M. van Griensven, W. Zhang, M.J. Coenen, C.V. Nagelli, J. A. Panos, C.J. Peniche Silva, J. Geiger, C. Plank, C.H. Evans, E.R. Balmayor, Efficient healing of large osseous segmental defects using optimized chemically modified messenger RNA encoding BMP-2, Sci. Adv. 8 (7) (2022) eabl6242.
[10] E.R. Balmayor, J.P. Geiger, M.K. Aneja, T. Berezhanskyy, M. Utzinger, O. Mykhaylyk, C. Rudolph, C. Plank, Chemically modified RNA induces osteogenesis of stem cells and human tissue explants as well as accelerates bone healing in rats, Biomaterials 87 (2016) 131–146.
[11] C. Del Toro Runzer, S. Anand, C. Mota, L. Moroni, C. Plank, M. van Griensven, E. Balmayor, Cellular uptake of modified mRNA occurs via caveolae-mediated endocytosis, yielding high protein expression in slow-dividing cells, Mol. Ther. Nucleic Acids 32 (2023).
[12] S.K. Both, A.J.v.d. Muijsenberg, C.A.v. Blitterswijk, J.d. Boer, J.D.d. Bruijn, A rapid and efficient method for expansion of human mesenchymal stem cells, Tissue engineering 13(1) (2007) 3-9.
[13] J. Schindelin, I. Arganda-Carreras, E. Frise, V. Kaynig, M. Longair, T. Pietzsch, S. Preibisch, C. Rueden, S. Saalfeld, B. Schmid, Fiji: an open-source platform for biological-image analysis, Nat. Methods 9 (7) (2012) 676–682.
[14] S. Qin, X. Tang, Y. Chen, K. Chen, N. Fan, W. Xiao, Q. Zheng, G. Li, Y. Teng, M. Wu, mRNA-based therapeutics: powerful and versatile tools to combat diseases, Signal Transduct. Target. Ther. 7 (1) (2022) 166.
[15] R.-M. Lu, H.-E. Hsu, S.J.L.P. Perez, M. Kumari, G.-H. Chen, M.-H. Hong, Y.-S. Lin, C.-H. Liu, S.-H. Ko, C.A.P. Concio, Current landscape of mRNA technologies and delivery systems for new modality therapeutics, J. Biomed. Sci. 31 (1) (2024) 89.
[16] R.O. Egberink, D.M. van Schie, B. Joosten, L.T. de Muynck, W. Jacobs, J. van Oostrum, R. Brock, Unraveling mRNA delivery bottlenecks of ineffective delivery vectors by co-transfection with effective carriers, Eur. J. Pharm. Biopharm. 202 (2024) 114414.
[17] A. El-Sayed, H. Harashima, Endocytosis of gene delivery vectors: from clathrin-dependent to lipid raft-mediated endocytosis, Mol. Ther. 21 (6) (2013) 1118–1130.
[18] C.D.T. Runzer, S. Anand, C. Mota, L. Moroni, C. Plank, M. van Griensven, E. R. Balmayor, Cellular uptake of modified mRNA occurs via caveolae-mediated endocytosis, yielding high protein expression in slow-dividing cells, Molecular Therapy-Nucleic Acids 32 (2023) 960–979.
[19] J. Rejman, V. Oberle, I.S. Zuhorn, D. Hoekstra, Size-dependent internalization of particles via the pathways of clathrin-and caveolae-mediated endocytosis, Biochem. J 377 (1) (2004) 159–169.
[20] B.B. Mendes, J. Conniot, A. Avital, D. Yao, X. Jiang, X. Zhou, N. Sharf-Pauker, Y. Xiao, O. Adir, H. Liang, Nanodelivery of nucleic acids, Nat. Rev. Methods Primers 2 (1) (2022) 24.
[21] R. Bilardo, F. Traldi, A. Vdovchenko, M. Resmini, Influence of surface chemistry and morphology of nanoparticles on protein corona formation, Wiley Interdiscip. Rev. Nanomed. Nanobiotechnol. 14 (4) (2022) e1788.
[22] C.H. Lohmann, Z. Schwartz, G. Köster, U. Jahn, G.H. Buchhorn, M. MacDougall, D. Casasola, Y. Liu, V. Sylvia, D. Dean, Phagocytosis of wear debris by osteoblasts affects differentiation and local factor production in a manner dependent on particle composition, Biomaterials 21 (6) (2000) 551–561.
[23] M.P. Stewart, A. Lorenz, J. Dahlman, G. Sahay, Challenges in carrier-mediated intracellular delivery: moving beyond endosomal barriers, Wiley Interdiscip. Rev. Nanomed. Nanobiotechnol. 8 (3) (2016) 465–478.
[24] A. Dirisala, S. Uchida, J. Li, J.F. Van Guyse, K. Hayashi, S.V. Vummaleti, S. Kaur, Y. Mochida, S. Fukushima, K. Kataoka, Effective mRNA protection by poly (l-ornithine) synergizes with endosomal escape functionality of a charge-conversion polymer toward maximizing mRNA introduction efficiency, Macromol. Rapid Commun. 43 (12) (2022) 2100754.
[25] L.D. Cervia, C.-C. Chang, L. Wang, F. Yuan, Distinct effects of endosomal escape and inhibition of endosomal trafficking on gene delivery via electrotransfection, PLoS One 12 (2) (2017) e0171699.
[26] T. Yoshimori, A. Yamamoto, Y. Moriyama, M. Futai, Y. Tashiro, Bafilomycin A1, a specific inhibitor of vacuolar-type H (+)-ATPase, inhibits acidification and protein degradation in lysosomes of cultured cells, J. Biol. Chem. 266 (26) (1991) 17707–17712.
[27] M. Tingey, S.J. Schnell, W. Yu, J. Saredy, S. Junod, D. Patel, A.A. Alkurdi, W. Yang, Technologies enabling single-molecule super-resolution imaging of mRNA, Cells 11 (19) (2022) 3079.
[28] M. Takatsu, K. Morihiro, H. Watanabe, M. Yuki, T. Hattori, K. Noi, K. Aikawa, K. Noguchi, M. Yohda, T. Okazoe, Cellular Penetration and Intracellular Dynamics of Perfluorocarbon-Conjugated DNA/RNA as a potential Means of Conditional Nucleic Acid delivery, ACS Chem. Biol. 18 (12) (2023) 2590–2598.